Thermal and Near-Thermal Reactions of Pt^+ and Au^+ with Small Alkenes

William S. Taylor,* Allyson S. Campbell, and Daniel F. Barnas

Department of Chemistry, University of Central Arkansas, Conway, Arkansas 72035

Lucia M. Babcock and Christopher B. Linder

Department of Chemistry, University of Georgia, Athens, Georgia 30602

Received: November 26, 1996; In Final Form: January 30, 1997[⊗]

The gas-phase reactions of Pt^+ and Au^+ with C_2H_4, C_3H_6, 1-C_4H_8, *cis*-2-C_4H_8, and *trans*-2−C_4H_8 have been carried out under thermal and near-thermal conditions using a SIFT reactor and a drift cell. In all reactions examined here, Pt^+ exhibits dehydrogenation as the dominant primary product channel, but elimination of methane and ethene are observed in some systems in small amounts. Evidence for both allylic and vinylic activation of σ-bonds is observed. Observation of these bimolecular processes allow us to calculate $D(Pt^+\cdot$acetylene$) > 49.76 \pm 0.01$ kcal/mol, $D(Pt^+\cdot$allene$) > 40.75 \pm 0.01$ kcal/mol, $D(Pt^+\cdot$propyne$) > 39.7 \pm 0.1$ kcal/mol and $D(Pt^+\cdot$butadiene$) > 29.01 \pm 0.01$ kcal/mol. Hydride abstraction is also observed as a minor product channel in the reactions of Pt^+ with C_3H_6 and all three butene isomers. Secondary and tertiary reactions in the Pt^+ systems are limited to clustering reactions. Hydride abstraction is the only primary bimolecular pathway observed in the reactions of Au^+ with propene as well as the butene isomers. Au^+ forms adducts with both C_2H_4 and C_3H_6 in primary steps. Follow-on reactions are also observed in the Au^+ systems which include both bimolecular and clustering steps. Ion mobility experiments carried out using the drift cell indicate that both Pt^+ and Au^+ are in their ground states in the reactions described here. However, we show evidence that an Au^+ excited state can be populated under the appropriate ionizing conditions. Reduced zero-field mobilities for ground-state Pt^+ and Au^+ have been determined to be 20.6 ± 0.6 and 19.5 ± 0.5 $cm^2/V\cdot s$, respectively.

Introduction

The gas-phase chemistry of bare metal ions has been the subject of a great deal of interest for more than a decade.[1−4] Of particular interest has been the activation of σ-bonds by metal ions, resulting in the production of other useful molecules. A large body of this work has focused on reactions involving hydrocarbons, in which oxidative addition to both C−H and C−C bonds has been observed. Studies of this nature are useful in understanding the behavior of organometallic intermediates in catalytic mechanisms and have provided valuable thermochemical and kinetic information regarding these species. The behavior of the first-row metal ions in these reactions has been studied extensively under single-collision conditions, as well as those in which three-body processes are possible. By comparison, fewer studies have focused on the chemistry of the third-row transition-metal ions. However, it has been shown that these ions exhibit considerably greater reactivity than their first- and second-row homologues as a result of stronger metal-ligand interactions arising from the similar sizes of the 5d and 6s orbitals.[5−12] Consequently, many third-row metals exhibit exothermic elimination chemistry not seen with ions of the first transition series. The work described here further illustrates differences as well as similarities in the behavior of these heavier ions to that of the first-row ions.

Alkenes represent one class of neutral reactant where the increased reactivity of the third-row ions has been observed. For example, ethene and propene exhibit exothermic bimolecular chemistry only with early first-row transition-metal ions,[4,13−15] whereas heavier ions readily eliminate H_2 from these neutrals.[9,16] In this work, we examine the gas-phase reactions of Pt^+ and Au^+ with ethene, propene, and linear butenes under thermal and near-thermal conditions. Since alkenes have the capability to form π-complexes with transition metals, adduct formation is possible under multicollisional conditions and is observed if no bimolecular channels are thermochemically or kinetically favorable. At the same time, the alkene provides a substrate with which the rich bimolecular chemistry of the third-row ions can be studied. The potential availability of both types of products affords us with the opportunity to examine factors influencing competition between adduct formation and other elimination channels.

In the reactions of first-row ions with alkenes, the metal initially associates itself with the π-bond, which can then be followed by activation of a C−C or C−H bond located elsewhere on the neutral. Complexation of the metal to multiple bonds is usually followed by activation of an allylic C−C or C−H bond,[13,15,17,18] but regiospecific activation of bonds remote to the multiple bond has also been observed.[19−21] Activation of an allylic C−C bond can result in the formation of a bis-olefin complex which can then undergo ligand detachment of the smaller, more weakly bound olefin under sufficiently energetic conditions.[17] Alternatively, allylic C−H bond activation results in dehydrogenation. This product channel predominates in reactions involving second- and third-row ions.[4,6,11] The presence of additional ligands bound to the metal has also been demonstrated to have a profound effect on access to available product channels.[9,14,15,22−25] Significant with respect to this work are previous observations in which the presence of π-ligands limits σ-bond activation by the metal. Similarly, the presence of π-ligands appears to strongly influence follow-on reactions in the processes involving Pt^+ described here. These ligand effects, as well as marked differences in the behavior of Pt^+ and Au^+ from each other and from that of earlier third-row metal ions, are consistent with the idea that σ-bond activation is less efficient as the d-orbitals become more populated.

[⊗] Abstract published in *Advance ACS Abstracts,* March 1, 1997.

S1089-5639(96)03927-8 CCC: $14.00

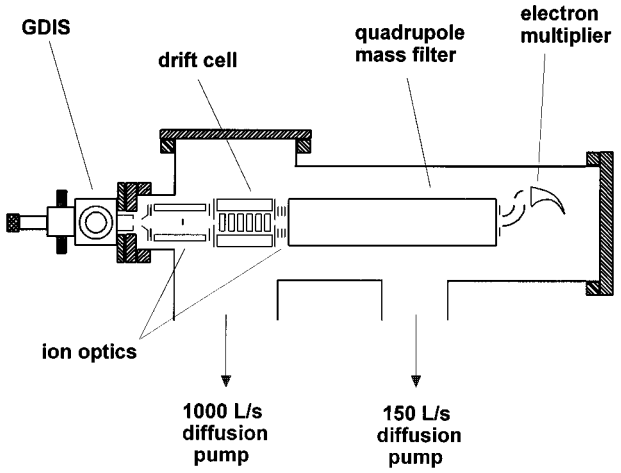

Figure 1. Diagram of instrument incorporating the glow discharge ion source (GDIS), drift cell, and quadrupole.

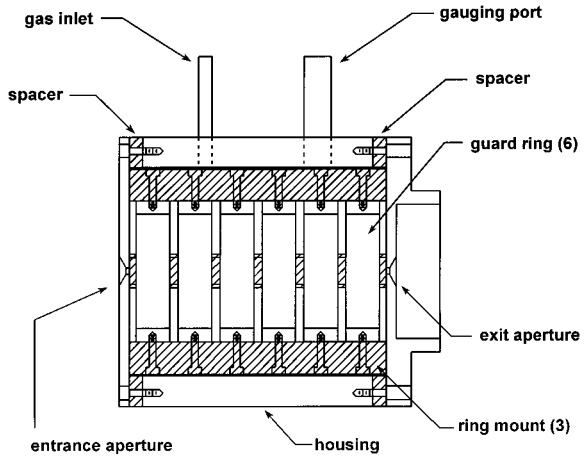

Figure 2. Detailed schematic of the drift cell.

Experimental Section

Reactions were carried out using two instruments. The first is a recently constructed drift cell reactor located at the University of Central Arkansas, and the second is a selected ion flow tube (SIFT) located at the University of Georgia which has been described in detail elsewhere.[26] In both instruments, metal ions were produced in a sputtering dc glow discharge. The drift cell reactor was constructed from a Delsi-Nermag R10-10C quadrupole mass spectrometer. This instrument is shown in Figure 1. The R10-10C was modified for this work by replacing the standard ionizer assembly with an ion optics array which incorporates the drift cell. The externally mounted dc glow discharge ion source and optics to transport the ions from the source were also added. The remaining pre- and postquadrupole optics were unaltered.

The drift cell is shown in greater detail in Figure 2. This device is similar to one which has been described previously[27] and consists of a cylindrical reaction volume 4.0 cm in length and 3.4 cm in diameter. Housed within this cylinder is a set of six guard rings connected in series to the entrance and exit plates by 1.5 MΩ resistors. The guard rings are supported within the drift cell housing by three ring-mounts fashioned from Torlon.[28] The drift cell housing, guard rings, and entrance and exit plates are all constructed from 304 stainless steel. The entrance and exit plates are isolated from the housing by Torlon spacers. The exit plate is designed to fit into the existing ionizer socket on the quadrupole housing on the R10-10C. In the reactions described here, the cell was filled to a pressure of 1 Torr with a mixture of He and the desired alkene at partial pressure ratios ranging from approximately 1000/1 to 10000/1.

In the drift cell studies, reactant ions were formed externally in the glow discharge and focused onto a 0.5 mm diameter aperture in the entrance plate. Potentials applied to the entrance and exit plates defined the drift voltage, *V*, and were controlled independently to establish a field gradient within the cell. The ions were then drawn through the reaction mixture by the electric field, during which time reaction occurred. Ions exited the drift cell via a 0.5 mm diameter aperture in the exit plate and were mass-analyzed with the quadrupole. Reactant and product ions were detected with a continuous dynode electron multiplier, the output of which was directed to an EG&G Model VT120 fast-counting preamplifier and then to an EG&G Turbo-MCS multichannel scalar. Mass spectral data were displayed on a laboratory computer via software supplied with the MCS. Pressures within the drift cell were monitored using an MKS model 122B Baratron capacitance manometer, and gas flows were regulated with MKS Model 1159B mass flow controllers.

For the reactions examined here, calibrated alkene/He mixtures were prepared by pressurizing an evacuated steel bulb to 1−2 Torr with the pure alkene and then bringing the total pressure up to approximately 3000 Torr with He. This mixture was concentrated enough in the alkene that when introduced into the drift cell, established pseudo-first-order conditions with respect to the reactant ion. The extent of reaction was controlled by variations in the alkene number density at a constant drift field of approximately 5 Td. This was accomplished using a method similar to one which has been described previously in which the alkene partial pressure is varied while maintaining a constant total pressure with He.[29] The progress of reaction was monitored by acquiring mass spectra at a number of different extents of reaction, and plotting reactant and product ion peak areas as a function of the reactant neutral number density. This procedure proved to be adequate for observing the course of the reaction; however, measurement of neutral reactant concentrations in this manner lacked the precision necessary for the determination of rate constants. This was most likely due to differences in the conductance of the He and the reactant neutral in and out of the drift cell. Accordingly, all rate data reported here were obtained using the SIFT.

In the SIFT studies, ions produced in the glow discharge were mass filtered, and the desired reactant ions were injected into the flowtube where they were entrained in He buffer gas at pressures ranging from 0.3 to 0.5 Torr. He flows were measured with an MKS Model 1159B mass flow controller and maintained in the range of 10−16 standard liters/min. The pressure in the flowtube was measured with an MKS Model 122AA Baratron capacitance manometer. Reactant ions traveled through a 150 cm thermalization zone during which they experienced many collisions with the buffer gas. Reactant neutral flows were monitored by measuring the pressure drop across a calibrated capillary tube. The reactant neutral was injected into the flowtube 29.8 cm upstream from the detection orifice, and the reaction was allowed to proceed for a time defined by the buffer gas velocity and the length of the reaction zone, after which the gas mixture was sampled with a quadrupole mass spectrometer.

As was the case with the drift cell, the extent of reaction for the SIFT experiments was controlled by variation of the reactant neutral concentration. Kinetic and product distribution information was obtained by monitoring ion signals as a function of added neutral reactant. Rate coefficients were obtained from first-order decays of primary (metal) ion signals. Rate coefficients are reproducible to ±10%. Product branching ratios

were calculated from product ion signals (corrected for mass discrimination effects) and are reproducible to ±5%. all data were obtained at ambient temperature (~25 °C).

Glow Discharge Ion Source. In both instrumental techniques employed here, metal ions were produced in an external dc glow discharge ion source (GDIS) which has been described previously.[30,31] This ionization method produces intense and stable metal ion currents by a sputter-bombardment process. The substance to be ionized serves as the cathode in the discharge, and the anode is the discharge cell housing, which is at ground potential. In the reactions described here, the discharge was pressurized to approximately 500 mTorr with Ar. Ions are sampled from the discharge plasma via a 0.60 mm orifice immersed in the plasma. This sampling orifice is located in an electrode which is electrically isolated from the discharge cell housing. Since the space potential in the discharge plasma is defined by the most positive electrode with which it is in contact, the potential at which the ions are formed can be controlled by the application of a positive voltage to the sampling orifice, which is electrically isolated from the discharge cell housing.[32] In the drift cell experiments, the orifice bias is related to an important experimental parameter known as the injection energy. This is defined as the difference between the potential on the sampling orifice and the voltage on the drift cell entrance plate. Injection energies in the drift cell experiments discussed here were on the order of 12−15 eV. Lower injection energies resulted in unacceptable attenuation of the ion beam. It has been demonstrated that the injection energy is rapidly dissipated by the drift cell bath gas;[27] however, evidence of some translational heating due to this injection energy was observed for the ions examined here. In the SIFT experiments, the injection energy is the kinetic energy possessed by the ions as they exit the SIFT quadrupole, which was approximately 20 V in these experiments. In the SIFT, the injection energy is completely dissipated within the thermalization zone of the flowtube before the neutral reactant is encountered.

Mobility determinations described in this work were carried out using a method described elsewhere in which a 10 μs pulse of the reactant ion was introduced into the drift cell pressurized to 0.5−2.2 Torr.[33] Ion pulses were generated by applying a voltage to the sampling orifice in the discharge for 10 μs using a Hewlett-Packard Model 214A pulse generator. Because transmission of the ions is very sensitive to the voltage placed on this electrode, this has the effect of shuttering the ion beam. The MCS is triggered simultaneously. The quadrupole was tuned to transmit only the reactant ion mass, and the signal was collected in time-of-flight mode by the MCS. Arrival time distributions (ATDs) were collected as a function of drift voltage. The centers of these ATD's were then plotted as a function of V^{-1}, and K was determined from the slope of this line. Reduced mobilities, K_0, were obtained in the usual fashion by correcting the measured values of K to 0 °C and 760 Torr.

Purities for Pt and Au used as sputter targets were 99.9% and 99.99% respectively. Platinum was obtained as 1.0 mm wire and gold as a 3.0 mm rod. All of the alkenes were obtained with purities of >99% and were used without further purification. This was also the case also for the 99.999% argon used as the discharge gas. Helium used as the drift cell buffer gas and in preparing calibrated gas mixtures was obtained with a purity of 99.9999% and was passed through a 13× molecular sieve prior to its use. He used in the SIFT experiments was purified by passing it through a liquid nitrogen cooled sieve trap prior to its introduction into the flowtube.

Results and Discussion

Reaction Energetics: Pt^+ and Au^+ Mobilities. The SIFT reactor represents an environment where, in the absence of any internal excitation of the reactant ions by the source, the reaction energetics are defined by the temperature of the reactor, which in this case was 298 K. All of the reactions carried out in the SIFT can therefore be characterized as thermal with regard to translational energy, with center-of-mass kinetic energies (KE_{cm}) of 0.04 eV at room temperature. On the other hand, the drift cell represents a system in which the reactant ions can be translationally excited if the drift field strength, E, is sufficiently high (or the He number density, N, sufficiently low). The drift cell conditions used here were such that $E/N \approx 5$ Td, which is considered to be in the low-energy regime for most ions;[34] however, examination of the mobilities of the relatively massive reactant ions studied here yielded evidence of some perturbation by the injection voltage. This being said, we note that the same general behavior for these systems was observed in both the drift cell and the SIFT. Since the SIFT is a thermalized reaction environment, observed products must be formed exothermically, indicating that translational heating in the drift cell is not significant.

Reaction energetics for the drift cell experiments were determined by first measuring the mobility, K, for the reactant ion, and then calculating the drift velocity, v_d, via eq 1.

$$\vec{v}_d = K\vec{E}$$

The drift field, E, is defined as V/z, where V is the potential difference between the drift cell entrance and exit plates, and z is the distance between them. The drift velocity was then used to calculate KE_{cm} using methods which have been described previously.[27,35]

Examination of the behavior of the reactant ion mobilities can also provide information regarding the sensitivity of the reaction energetics of these heavy ions on drift cell conditions. Equation 1 applies only at low field strengths and describes drift velocity as a linear function of the drift field. Thus, if weak-field conditions exist, v_d should be a linear function of E, and K should be insensitive to variations in E/N. To test this, ion mobilities in He were determined over a range of field strengths and He number densities such that E/N values ranged from 1.8 to 26 Td. For a given value of N, i.e., a given pressure, plots of arrival time vs V^{-1} exhibited good linear behavior, indicating that K is not a function of E over the range of drift voltages examined (approximately 10 V at each pressure). However, Figure 3 clearly illustrates a marked dependance of "apparent K_0" on the value of N. For both Au^+ and Pt^+, values of apparent K_0 decreased as N increased, and approached a constant value at higher He number densities. Similar measurements using Ar^+ revealed the same behavior, except that a constant K_0 value is achieved at lower He number densities. This behavior is consistent with an "injection effect", in which residual injection energy influences the residence time of the ions in the drift cell.[27] Using the same criteria set forth by Kemper and Bowers, approximately 200 collisions are necessary to reduce our injection energy to 10% of thermal at 300 K for a 200 u ion in He.[27] By comparison, Ar^+ requires only 50 collisions to dissipate the same injection energy. This means that for a given injection voltage, the more massive the ion (and the lower the He pressure in the drift cell) the greater the influence of the injection energy on the residence time, t_R, and thus KE_{cm}. Examination of ion residence times as a function of injection energy confirms that this effect does occur, although the dependence is not strong at a drift cell pressure of 1 Torr

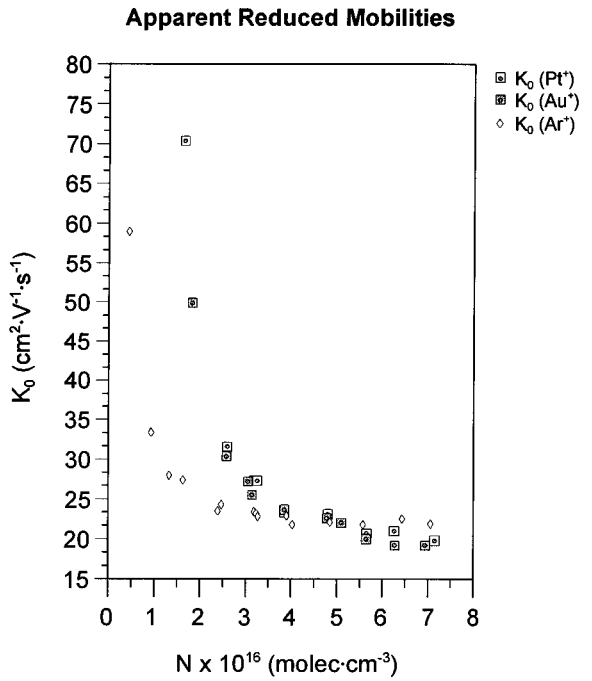

Figure 3. Apparent reduced zero-field mobilities for Ar^+, Pt^+, and Au^+ as a function of He number density in the drift cell. All measurements carried out at 300 K.

(the pressure used for the alkene reactions). In tests using platinum ions and drift cell conditions identical with those used in the reactions examined here, an increase in the injection voltage from 10 to 27 V resulted in a reduction in t_R of approximately 10%.

As is shown in Figure 3, experimental reduced mobilities for Pt^+ and Au^+ approach constant values at higher pressures. Measurement of K_0 at pressures above 2 Torr yields values of 20.6 ± 0.6 and 19.5 ± 0.5 $cm^2/V\cdot s$ for Pt^+ and Au^+, respectively, and we report these as the actual reduced zero-field mobilities for these species. These values are similar in magnitude to the reduced zero-field mobility which has been reported for Hg^+ in He.[36] The K_0 for Pt^+ is representative of an isotopic average, as it was obtained at low quadrupole resolution such that all isotopes were transmitted to the detector. The constant K_0 for Ar^+ of 22.2 ± 0.5 $cm^2/V\cdot s$ is also within experimental error of values reported previously for this ion in He.[33,37] To ensure that the presence of the alkene in the drift cell was not a perturbing factor, mobility measurements were carried out with He/alkene mixes where the alkene number densities were similar to those present at low extents of reaction. These determinations indicated that at the low mole fractions of alkene used here, the Au^+ and Pt^+ mobilities were not significantly affected.

Since the alkene reactions were carried out at pressures of 1 Torr, the apparent reduced mobilities of 27.4 and 25.6 $cm^2/V\cdot s$ for Pt^+ and Au^+ were used to determine the translational energetics of each reaction. As a result, KE_{cm} values were elevated slightly above that of thermal interactions—ranging from 0.05 eV when C_2H_4 was the reactant neutral to 0.07 eV for the C_4H_8 isomers. Attempts to lower interaction energies by reducing the drift field resulted in insufficient ion signals to carry out the reactions.

Electronically Excited Ions. It has been well documented that access to specific product channels is strongly influenced by the electronic configuration of the transition-metal ion.[3,38−42] This is apparent in comparisons of the reactions of metal ions within a transition series, as well as those of a given metal ion in different electronic states. Thus, an examination of the chemistry of Pt^+ and Au^+ requires us to first determine the extent to which excited states are populated by the glow discharge.

We have previously demonstrated that the GDIS is sufficiently energetic to populate one or more excited states of Co^+.[30] In this work, several metal ions (including Pt^+ and Au^+) produced in the GDIS were examined using a specific application of the mobility experiment described previously known as ion chromatography (IC).[33,43,44] This technique distinguishes between different electronic configurations of the same ion on the basis of differences in their mobilities and has been characterized primarily for the first-row metal ions. IC has been shown to be most effective in distinguishing between states which differ by the presence of an s electron. The larger size of the s orbital results in a greater repulsive interaction between the ion and the neutral bath gas. In terms of the first-row ions, this means that ions with $3d^{n-1}4s^1$ configurations have higher mobilities in the bath gas than ions with $3d^n$ configurations. As a consequence of the differences in their mobilities, a pulse containing $3d^{n-1}4s^1$ ions will exhibit a shorter arrival time to the electron multiplier than that of a pulse of $3d^n$ ions of the same mass-to-charge ratio. If the pulse contains ions of both configurations, they are temporally separated and appear as different peaks when the signal is collected in time-of-flight mode.

Initial IC experiments were carried out on Co^+, Ni^+, Cu^+, and Zn^+. The purpose for these determinations was to compare our IC results with those published previously for first-row ions[33] and to begin to establish the range of excited states accessible to the GDIS. Pulse widths employed here were on the order of 3−5 μs, and values of E/N ranged from 5 to 11 Td. All IC determinations were carried out at room temperature. Results of IC determinations on the four ions listed above indicate that all except Zn^+ are formed in at least one excited state in addition to the ground state. In all cases, configuration assignments were made on the basis of K_0 values, which were in good agreement those in the literature.[33] No published value for the reduced zero-field mobility was available for comparison for $Cu^+(3d^9 4s^1)$; however, this is the configuration for the ^3D first excited term for Cu^+, which lies 2.8 eV above the ground state. Further, our measured K_0 value for this species (21.8 ± 0.9 $cm^2/V\cdot s$) is close to that of the $3d^{n-1}4s^1$ configurations for other late first-row ions. Comparison of the ATDs for Co^+, Ni^+, and Cu^+ suggests that for a given set of discharge conditions, the relative amount of the more mobile excited state is greatest for Co^+ and least for Cu^+. This behavior correlates with the ordering of the energies required to achieve the $3d^{n-1}4s^1$ electronic configurations for these ions which are 0.43, 1.1, and 2.8 eV for Co^+, Ni^+, and Cu^+, respectively. For Cu^+ produced in an Ar discharge, excited-state production represents 10% or less of the total copper ion signal (dependent upon discharge conditions), which suggests that excited-state production in this environment is limited to those states which lie within approximately 3 eV of the ground state of the ion.

Excited state production for Co^+, Ni^+, and Cu^+ exhibits a dependence on discharge parameters—most notably discharge gas pressure and composition. In the case of Cu^+ produced in a pure Ar discharge, the percentage of the $3d^9 4s^1$ excited state configuration can be reduced to essentially zero by increasing the Ar pressure from 0.4 to 0.6 Torr. The opposite effect is observed when He is introduced into the discharge. As the proportion of He in the working gas increases, the fraction of excited state increases until, in a pure He discharge it represents approximately 34% of the total Cu^+ signal. This effect is

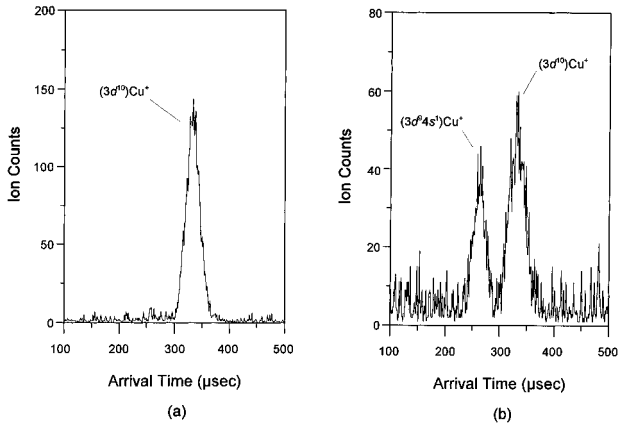

Figure 4. Arrival time distributions for Cu^+ produced in (a) a pure Ar discharge and (b) a pure He discharge. $T = 300$ K.

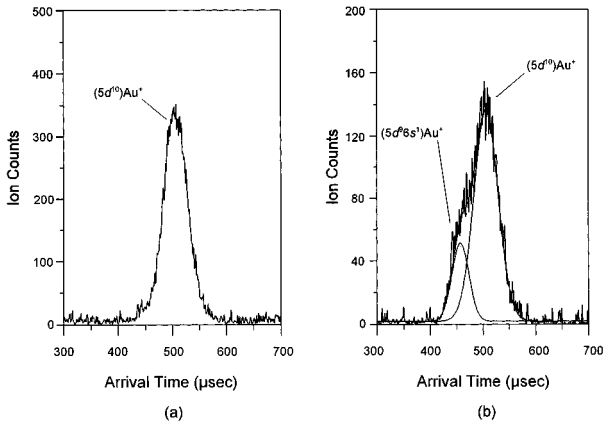

Figure 5. Arrival time distributions for Au^+ produced in (a) a pure Ar discharge and (b) a pure He discharge. $T = 300$ K.

illustrated in Figure 4. These observations suggest that the excited states are collisionally relaxed within the discharge.

IC analysis of Pt^+ and Au^+ ions produced in the GDIS were carried out at $E/N = 3$ Td. These results indicate that excited-state configurations of these ions are not significantly populated under the conditions employed in the reactions described here. The $^3D(5d^96s^1)$ state of Au^+ lies 2.5 eV above the ground state (averaged over J levels) and is the only excited-state configuration which falls within the range of energies accessible to the GDIS based on the first-row ion results. IC analysis of 5d ions is complicated by the fact that the chromatographic resolution of the third-row ATDs is poorer than that of the first-row ions under the same drift cell conditions. This is a result of the similar sizes of the 6s and 5d orbitals, which reduces the differences in the mobilities of the configurations. In addition, flight times through the instrument are longer for heavy ions than for lighter ones. As a result, the ion pulse is broadened, which further degrades chromatographic resolution. These factors introduce the possibility that excited states are present but unresolved. To determine the extent to which higher mobility Au^+ configurations can be resolved, ATDs were again obtained using both a pure Ar discharge and a pure He discharge. These are shown in Figure 5, where a shoulder is clearly visible in the pure He ATD which is absent in the pure Ar ATD. As is shown in Figure 5b, the Au^+/He ATD is well-represented by the sum of two Gaussians, indicating the presence of a more mobile configuration in addition to the $^1S(5d^{10})$ ground state. Given the behavior of Cu^+, we conclude that the higher mobility species is the $^3D(5d^96s^1)$ excited state of Au^+. We estimate the K_0 for the $5d^96s^1$ configuration at 22 $cm^2/V\cdot s$ based on the differences in the arrival times of the two species. This value is essentially the same as the K_0 we have reported for the $^3D(3d^94s^1)$ state of Cu^+ and seems quite reasonable in light of the fact that 6s and 4s orbitals are similar in size.[45] Since a pure Ar discharge was used in the alkene studies, reaction outcomes reported here reflect the behavior of ground-state Au^+. Further, no charge exchange products were observed in any of the reactions involving Au^+. Since charge exchange is energetically possible from the ^3D state but not the ^1S state, this also indicates that only the ground state was present at the time of reaction.

TABLE 1: Observed Reaction Products

reaction	primary prods	sec prods	tert prods	branching %[a]
$Pt^+ + C_2H_4$	$PtC_2H_2^+$	$PtC_4H_6^+$	$PtC_6H_{10}^+$	100
$Pt^+ + C_3H_6$	$PtC_3H_4^+$	$PtC_6H_{10}^+$	$PtC_9H_{16}^+$	>95
	$PtC_2H_2^+$			detected
	$C_3H_5^+$			detected
$Pt^+ +$ butenes	$PtC_4H_6^+$	$PtC_8H_{14}^+$	$PtC_{12}H_{22}^+$	>95
	$PtC_3H_4^+$			detected
	$PtC_2H_4^+$			detected
	$C_4H_7^+$			detected
$Au^+ + C_2H_4$	$AuC_2H_4^+$	$AuC_4H_8^+$	$AuC_6H_{12}^+$	100
$Au^+ + C_3H_6$	$AuC_3H_6^+$	$AuC_6H_{12}^+$		detected
	$C_3H_5^+$	$C_4H_7^+$	$C_7H_{13}^+$	>95
		$C_6H_{11}^+$		
$Au^+ +$ butenes	$C_4H_7^+$	$C_5H_9^+$	$C_9H_{17}^+$	100
		$C_8H_{15}^+$		

[a] Percentages indicate branching for primary product channels ±5%. Channels listed as "detected" are <5%.

Potentially accessible excited terms for Pt^+ include the ^4F, ^4P, and ^2F states, all of which have the $5d^86s^1$ configuration and are expected to be indistinguishable from one another via IC. These states lie 1.3, 2.5, and 2.6 eV (again averaged over J levels) above the ground state for this ion, respectively. A pure Ar discharge resulted in a symmetrical ATD for $^{195}Pt^+$ comparable to that of Au^+. Although not conclusive, this suggests that little or no Pt^+ $5d^86s^1$ configurations were sampled from the pure Ar discharge utilized in the alkene reactions. A pure He discharge yielded insufficient Pt^+ signal for IC analysis. Consideration must also be given to the two J states within the ground state ^2D term, ($^2D_{5/2}$ and $^2D_{3/2}$) which are split by 1.0 eV. These two spin−orbit states would also be indistinguishable from one another in the IC experiment; thus, population of the $^2D_{3/2}$ J level would not be detected in this manner. However, we again note that no charge-exchange (endothermic from the $^2D_{5/2}$ state) was observed in reactions of this ion with the alkenes discussed below, suggesting that no excited Pt^+ is present at the time of reaction. Finally, the kinetic results and product distributions obtained in the SIFT experiments indicate either that only one reactive Pt^+ state is populated or that differences in their reactivities are insignificant. Both the IC result and SIFT observations could also simply be an indication that excited Pt^+ configurations are being rapidly deactivated prior to reaction.

Alkene Reactions. A summary of the observed products of these reactions is given in Table 1. These data clearly illustrate the differences in the behavior of the two metal ions. Pt^+ displays a variety of bimolecular product channels with the alkenes studied here. H_2 elimination is the dominant process, but minor product channels are observed in some systems for hydride abstraction, loss of CH_4, and loss of C_2H_4. These minor products were observed in the SIFT and not in the drift cell due either to isobaric interferences or low signal intensities. For Pt^+, adduct formation is observed only in follow-on reactions. By contrast, Au^+ displays primary adduct formation in reaction with both C_2H_4 and C_3H_6. The bimolecular chemistry of Au^+ is limited to hydride abstraction.

TABLE 2: Second-Order Rate Constants for the Reactions of Pt^+ and Au^+ with C_2H_4, C_3H_6, and C_4H_8 Isomer[a]

reaction	k_{obs} ($\times 10^{-10}$)	k_{coll} ($\times 10^{-10}$)	k_{obs}/k_{coll}
$Pt^+ + C_2H_4$	9.4	9.7	0.97
$Pt^+ + C_3H_6$	11	10.7	1.0
$Pt^+ + 1\text{-}C_4H_8$	11	10.6	1.0
$Pt^+ + c\text{-}2\text{-}C_4H_8$	9.4	9.9	0.95
$Pt^+ + t\text{-}2\text{-}C_4H_8$	10	10.3	0.97
$Au^+ + C_2H_4$	6.5	9.7	0.67
$Au^+ + C_3H_6$	9.8	10.6	0.93
$Au^+ + 1\text{-}C_4H_8$	11	10.6	1.0
$Au^+ + c\text{-}2\text{-}C_4H_8$	9.2	9.9	0.93
$Au^+ + t\text{-}2\text{-}C_4H_8$	10	10.3	0.97

[a] Rate constants in units of $cm^3 \cdot molecule^{-1} \cdot s^{-1}$.

Overall second-order rate constants, k_{obs}, measured using the SIFT are given in Table 2. Comparison of these values with the collision limit rate constant, k_{coll}, obtained from parametrized trajectory calculations[46] indicate that all but one of the reactions examined here are proceeding at or slightly below the collision limit. The exception to this is the Au^+/ethene system, which exhibits association chemistry exclusively. The apparent bimolecular rate constant for this process represents approximately 67% of the collision limit over a 0.38−0.70 Torr pressure range, and displays a weak pressure dependance. The average three-body rate constant for this reaction is 3.9×10^{-26} $cm^6 \cdot molecules^{-2} \cdot s^{-1}$.

Ethene Reactions. Reaction of Pt^+ with C_2H_4 results in the formation of a $Pt^+ \cdot C_2H_2$ species via H_2 elimination. Since all C−H bonds are equivalent in this alkene, H_2 elimination must occur via activation of a vinylic C−H bond. This is presumably followed by β-hydrogen migration to form a dihydrido−Pt−acetylene intermediate from which H_2 is subsequently lost, resulting in the $Pt^+ \cdot C_2H_2$ ionic product. A $Pt^+ \cdot$acetylene structure is proposed for the primary product rather than a $Pt^+ \cdot$dicarbene species based on structures for analogous complexes containing Sc^+, Nb^+, and Ta^+.[10,11,15] Secondary and tertiary association reactions are also observed. While H_2 elimination has been observed for the reaction of Sc^+ and V^+ with C_2H_4,[4,15] this alkene exhibits no exothermic chemistry with late first-row metal ions. The behavior of Pt^+ exhibited here further illustrates the greater reactivity of the third-row metal ions in comparison to their first-row homologues; however, Pt^+ does not appear to be as reactive as ions earlier in the same period. Whereas Pt^+ is observed here to eliminate H_2 once from C_2H_4, Os^+ is known to dehydrogenate C_2H_4 in both primary, secondary, and tertiary steps.[9]

Reaction of Au^+ with C_2H_4 yields a primary adduct, which is subsequently consumed in a secondary clustering step. A tertiary clustering step is observed only in the drift cell, which operates at a higher He pressure than the SIFT. Previously reported ligand-switching experiments suggest that the $Au^+ \cdot C_2H_4$ structure contains a π-bound ethene ligand,[8] and a recent theoretical examination of this species predicts a metallacyclopropane structure.[47] Hydride abstraction to form AuH is endothermic with this alkene from $Au^+(^1S)$ and is not observed under the energetic conditions utilized here.

Propene Reactions. Reaction of Pt^+ with this hydrocarbon exhibits H_2 elimination as the major primary product channel resulting in formation of $Pt^+ \cdot C_3H_4$. This is followed by secondary and tertiary clustering steps. Possible ionic dehydrogenation products are either a $Pt^+ \cdot$allene structure or a $Pt^+ \cdot$propyne species. No experiments were carried out here to determine if either (or both) of these structures were present; however, elimination of H_2 has also been observed in the reactions of Sc^+, Gd^+, and Pr^+ with propene, in which the resulting $M^+ \cdot C_3H_4$ species has been proposed to contain the allene ligand.[15,48] If the $Pt^+ \cdot C_3H_4$ species in our experiments likewise incorporates the allene ligand, $D(Pt^+-C_3H_4) > 40.75 \pm 0.01$ kcal/mol is indicated, whereas a $Pt^+ \cdot$propyne structure would imply $D(Pt^+-C_3H_4) > 39.7 \pm 0.1$ kcal/mol.

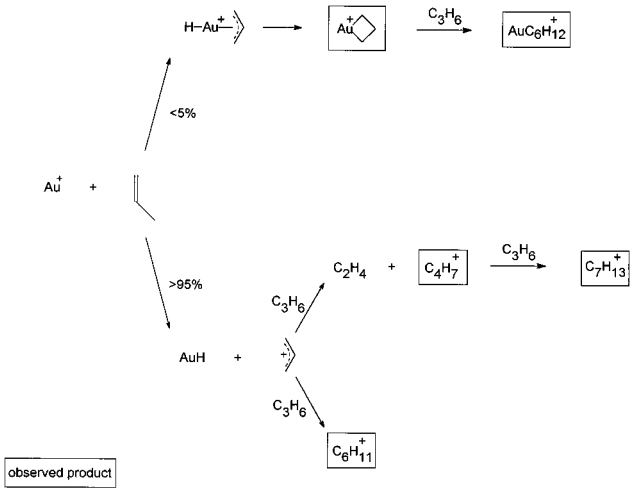

Figure 6. Proposed scheme describing the reaction of Au^+ with C_3H_6.

Evidence of C−C bond activation is indicated by the formation of $Pt^+ \cdot C_2H_2$ as a minor product. Generation of this species could occur via vinylic C−C bond activation followed by β-hydrogen migration and reductive elimination of CH_4. Similar behavior has been seen in the reaction of propene with Co^+.[49] Alternatively, vinylic C−H activation with subsequent β-methyl migration could occur; however, it has been argued that the latter would be less favorable due to the directional nature of the orbitals in the migrating methyl group.[10] In either case, observation of the $Pt^+ \cdot C_2H_2$ fragment in this system implies $D(Pt^+-C_2H_2) > 49.76 \pm 0.01$ kcal/mol. This lower limit is close to that which has been established previously for $M^+-C_2H_4$ π-complexes[10] and seems reasonable since the interaction of the π cloud of acetylene with the metal center should be similar to that of ethene. Production of PtH via hydride abstraction is exothermic by 24 kcal/mol in this system, but $C_3H_5^+$ is observed only as a minor product, indicating that H_2 elimination is the kinetically favored process.

Primary reaction channels in the reaction of Au^+ with C_3H_6 include hydride abstraction, which is exothermic by 18.5 kcal/mol, as well as a minor contribution from adduct formation. These processes are summarized in Figure 6. With the exception of some cluster formation observed in our experiments at high extent of reaction in the drift cell, the behavior of this system is consistent with that observed previously, in which a metallacyclobutane structure has been suggested for the adduct.[8] This structure implies allylic C−H bond activation and, if occurring, is the only instance of C−H bond activation exhibited by Au^+ with any of the alkenes examined here. The primary product of hydride abstraction is presumed to be the allyl cation, $C_3H_5^+$, which is itself consumed in two parallel secondary reactions with C_3H_6. The first of these eliminates C_2H_4, yielding $C_4H_7^+$, which is subsequently consumed in a tertiary clustering step with C_3H_6. Allyl cation also clusters with C_3H_6 to yield $C_6H_{11}^+$. As in the Au^+/ethene system, the primary $Au^+ \cdot C_3H_6$ species exhibits secondary clustering with C_3H_6. No tertiary clusters were observed in this system, possibly due to low signal intensities.

Butene Reactions. Reaction of Pt^+ with 1-butene, and the two 2-butene isomers exhibits H_2 elimination to yield $Pt^+ \cdot C_4H_6$ as the predominant primary product channel. Minor product channels include CH_4 loss, C_2H_4 loss, and hydride abstraction. The elimination products observed in these systems can be

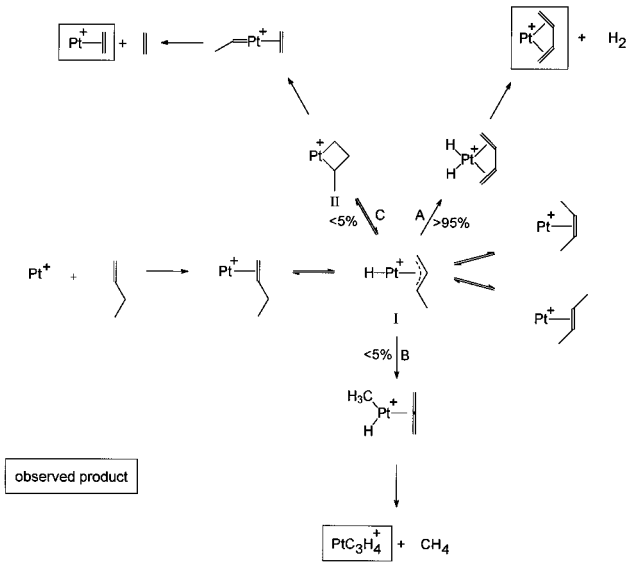

Figure 7. Proposed scheme describing the reaction of Pt^+ with linear butenes.

explained by a number of different mechanistic pathways which differ in the identity and position of the bond which is initially activated. Taken together, all of these mechanistic possibilities result in a complex picture of the behavior of these reactions; however, the propensity of the third-row ions to activate C−H bonds preferentially suggests that the steps outlined in Figure 7 are the most likely. Here, as in previous studies,[13,15] the equivalent behavior of all three butenes is consistent with the existence of an equilibrium between the platinum complexes of all three linear butenes. This equilibrium is established as a result of facile hydrogen migration via the common hydrido π-allylplatinum intermediate (**I**), which is formed by allylic C−H bond activation. Dehydrogenation has been observed in the reactions of a number of other metal ions with linear butenes, in which a butadiene structure is proposed for the ligand in the ionic product.[13−15,48,50] Production of the Pt^+·butadiene structure occurs from **I** via path A, in which β-hydrogen migration to the platinum center is followed by loss of H_2. Dehydrogenation is least exothermic with *trans*-2-butene and thus allows us to establish $D(Pt^+-\text{butadiene}) > 29.01 \pm 0.01$ kcal/mol. As in the ethene and propene systems, no further dehydrogenations are observed after formation of the primary product. Rather, secondary and tertiary clusters are formed from subsequent reaction of $Pt^+ \cdot C_4H_6$ with all three butenes.

Production of $Pt^+ \cdot C_3H_4$ occurs via β-methyl migration in **I** (path B), followed by reductive elimination of CH_4, while loss of C_2H_4 can occur in a manner analogous to that proposed previously in reactions involving Co^+.[13,49] In this scheme, a methyl metallacycle (**II**) is formed via path C, which is again accessible to all three butene isomers via **I**. Subsequent rearrangement results in the production of $Pt^+ \cdot C_2H_4$. The product spectrum in this reaction also contains evidence suggesting that a small amount of a species with a mass corresponding to that of $Pt^+ \cdot C_2H_2$ may also be formed. This species would result from elimination of C_2H_6; however, the ion signal was of such low intensity that it could not be conclusively resolved from the $Pt^+ \cdot C_2H_4$ peak.

Reactions of all three butenes with Au^+ results exclusively in hydride abstraction to yield $C_4H_7^+$ as a primary product. Secondary and tertiary reactions are analogous to those described for the Au^+/propene system. Here, $C_4H_7^+$ reacts in two competing secondary steps to yield $C_5H_9^+$ (via loss of C_3H_6) and $C_8H_{15}^+$ (via association with C_4H_8). The $C_5H_9^+$ product also participates in a clustering step with C_4H_8 to yield $C_9H_{17}^+$.

Finally, we note that charge exchange is very nearly thermoneutral in the reactions of ground-state Au^+ with both of the 2-butenes. Product ions were observed at the limit of detection which could result from follow-on reactions of $C_4H_8^+$; however, no *direct* evidence of charge-exchange was observed.

Ligand Effects. Pt^+ induces elimination of H_2 with all alkenes examined here exclusively in primary steps. The resulting $Pt^+ \cdot C_nH_{2n-2}$ complex is apparently "deactivated" with respect to further H_2 eliminations as evidenced by the observation of only association products in follow-on steps. This ligand effect has also been documented in the reactions of Ni^+ with linear butenes, in which the primary $Ni^+ \cdot$butadiene species is significantly reduced in its reactivity in comparison with the bare ion.[14] Similarly, the presence of π-ligands has been shown to limit σ bond activation by Fe^+ and FeO^+.[22−24,50] The deactivating influence of these π-ligands is understood by considering that σ-bond activation involves the formation of a "donor−acceptor complex" in which the metal accepts electron density from the bond, while at the same time back-donating electron density into the σ^* orbital. The "acceptor" character of the metal is known to have a significant effect on its ability to participate in oxidative addition. For first-row metals, it has been illustrated that larger 4s orbital serves a larger role in withdrawing electron density from the activated σ-bond than the 3d orbitals and that oxidative addition proceeds less efficiently when the 4*s* orbital is occupied.[3,38] The similar sizes of the 5d and 6s orbitals in the third row allow 5d orbitals or sd hybrids of the appropriate symmetry to also accept electron density in σ-bond activation. Thus, the degree to which these orbitals are populated is expected to also be an influence on σ-bond activation for these heavier ions. The binding of π-ligands to transition metals is characterized by donation of electron density from the π cloud of the ligand to the metal as well as back donation by the metal into the π^* ligand orbital. Our results, as well as those cited for Ni^+ and Fe^+ indicate that electron donation to the metal in these is the more significant effect, and the reduction in the Lewis acidity of the metal precludes further C−H bond activation by reducing its ability to accept electrons from the σ-bond. This is further illustrated by the behavior of different ions within the period. Pt^+ ($5d^9$) participates in a single dehydrogenation step with all the alkenes examined here, whereas Au^+ ($5d^{10}$) exhibits no C−H bond activation with the same neutrals. Interestingly, Os^+ ($5d^66s^1$) has been observed to induce three H_2 eliminations in reactions with successive C_2H_4 molecules,[9] and Ta^+($5d^36s^1$) is known to participate in multiple dehydrogenation steps, although ligand-coupling may be occurring as well in this case. This further illustrates the greater role of the 5d orbitals in activating σ-bonds in these heavier metal ions. This is also consistent with the small amount of C−C bond cleavage observed here, which is thought to occur most efficiently when the participating metal orbitals are nondirectional, which is not the case for the d orbitals.[10] The above comparisons clearly support the idea that the "sparseness" of the 5d orbitals has a dramatic effect on dehydrogenation.

Summary

The chemistry of Pt^+ and Au^+ with several alkenes has been examined. Using ion chromatography, both ions have been determined to be formed in their ground states in a sputtering argon glow discharge. These results indicate that the low energy interactions of ground state Pt^+ with small alkenes are dominated by C−H bond activation resulting in dehydrogenation. This

occurs as a result of vinylic C−H bond activation in the case of ethene, and most likely allylic C−H bond activation when propene and linear butenes are the reactant neutrals. Further, the reactions of Pt^+ with propene and linear butenes all exhibit evidence of several other minor elimination product channels. Inefficient hydride abstraction is also observed to occur in the Pt^+ systems when it is energetically favorable. Reactions of ground-state Au^+ exhibit hydride abstraction as the only bimolecular product channel; however, C−H bond activation may occur in the reaction of Au^+ with C_3H_6 to form the adduct. Adduct formation is observed only in follow-on reactions in the Pt^+ systems and with ethene and propene only when Au^+ is the reactant ion. Follow-on reactions in the Pt^+ systems exhibit a ligand effect which suggests that electron donation from the ligand π-orbital reduces the Lewis acidity of the metal to the point where further oxidative addition is inhibited.

Acknowledgment. The authors wish to gratefully acknowledge the financial support of this work by Research Corp. under Grant C-3472 and the donors of the Petroleum Research Fund administered by the American Chemical Society under Grant 30312-3B. We also wish to acknowledge the support of the National Center for Toxicological Research in Jefferson, Arkansas, in providing instrumentation used in the construction of the drift cell reactor.

References and Notes

(1) Armentrout, P. B.; Beauchamp, J. L. *Acc. Chem. Res.* **1989**, *22*, 315−321.
(2) Weisshaar, J. C. *Acc. Chem. Res.* **1993**, *26*, 213−219.
(3) Armentrout, P. B. *Annu. Rev. Phys. Chem.* **1990**, *41*, 313−344.
(4) Eller, K. E.; Schwarz, H. *Chem. Rev.* **1991**, *91*, 1121−1177.
(5) Ward, E. E.; Taylor, W. S.; Babcock, L. M.; McNeal, T. L. *Proceedings of the 41st ASMS Conference on Mass Spectrometry and Allied Topics*; San Francisco, CA, May 30−June 1, 1993; p 169.
(6) Eller, K; Schwarz, H, *Chem. Ber.* **1990**, *123*, 201−208.
(7) Weil, D. A.; Wilkins, C. L. *J. Am. Chem. Soc.* **1985**, *107*, 7316−7320.
(8) Chowdhury, A. K.; Wilkins, C. L. *J. Am. Chem. Soc.* **1987**, *109*, 5336−5343.
(9) Irikura, K. K.; Beauchamp, J. L. *J. Am. Chem. Soc.* **1989**, *111*, 75−85.
(10) Irikura, K. K.; Beauchamp, J. L. *J. Phys. Chem.* **1991**, *95*, 8344−8351.
(11) Buckner, S. W.; Macmahon, T. J.; Byrd, G. D.; Freiser, B. S. *Inorg. Chem.* **1989**, *28*, 3511−3518.
(12) Dance, I. G.; Fisher, K. J.; Willet, G. D. *Inorg. Chem.* **1996**, *35*, 4177−4184.
(13) Armentrout, P. B.; Halle, L. F.; Beauchamp, J. L. *J. Am. Chem. Soc.* **1981**, *103*, 6624−6628.
(14) Hettich, R. L.; Freiser, B. S. *Organometallics* **1989**, *8*, 2447−2453.
(15) Lech, L. M.; Freiser, B. S. *Organometallics* **1988**, *7*, 1948−1957.
(16) Cassady, C. J.; McElvany, S. W. *J. Am. Chem. Soc.* **1990**, *112*, 4788−4797.
(17) Peake, D. A.; Gross, M. L.; Ridge, D. P. *J. Am. Chem. Soc.* **1984**, *106*, 4307−4315.
(18) Peake, D. A.; Gross, M. L. *J. Am. Chem. Soc.* **1987**, *109*, 600−602.
(19) Schultz, C.; Schwarz, H.; Peake, D. A.; Gross, M. L. *J. Am. Chem. Soc.* **1987**, *109*, 2368−2374.
(20) Schwarz, H. *Acc. Chem. Res.* **1989**, *22*, 282−287.
(21) Schulze, C.; Schwarz, H. *J. Am. Chem. Soc.***1988**, *110*, 67−70.
(22) Stöckigt, D.; Sen, S.; Schwarz, H. *Chem. Ber.* **1993**, *126*, 2553−2557.
(23) Schröder, D.; Eller, K.; Prüsse, T; Schwarz, H. *Organometallics* **1991**, *10*, 2052−2055.
(24) Stöckigt, D.; Schwarz, H. *Chem. Ber.* **1994**, *127*, 2499−2503.
(25) Tjelta B. L.; Armentrout, P. B. *J. Am. Chem. Soc.* **1995**, *117*, 5531−5533.
(26) Babcock, L. M.; Taylor, W. S.; Linder, C. B. In *Advances in Gas Phase Ion Chemistry*; Adams, N. G., Babcock, L. M. Eds.; JAI Press Inc.: Greenwich, CT; Vol. 3, in press.
(27) Kemper, P. R.; Bowers, M. T. *J. Am. Soc. Mass Spectrom.* **1990**, *1*, 197−207.
(28) Torlon is a registered trademark of Amoco Polymers Inc.
(29) Guo, B. C.; Kerns, K. P.; Castleman, A. W. *J. Phys. Chem.* **1992**, *96*, 4879−4883.
(30) Taylor, W. S.; Everett, W. R.; Babcock, L. M.; McNeal T. L. *Int. J. Mass Spectrom. Ion Proc.* **1993**, *125*, 45−54.
(31) Harrison, W. W.; Bentz, B. L. *Prog. Anal. Spectrosc.* **1988**, *11*, 53−110.
(32) Taylor, W. S.; Dulak, J. G.; Ketkar, S. N. *J. Am. Soc. Mass Spectrom.* **1990**, *1*, 448−454.
(33) Kemper, P. R.; Bowers, M. T. *J. Phys. Chem.* **1991**, *95*, 5134−5146.
(34) Mason, McDaniel, *Transport Properties of Ions in Gases*, Wiley, New York, 1988.
(35) McFarland, M.; Albritton, D. L.; Fehsenfeld, F. C.; Ferguson, E. E.; Schmeltekopf, A. L. *J. Chem. Phys.* **1973**, *59*, 6620−6628.
(36) McDaniel, E. W.; Mason, E. A. *The Mobility and Diffusion of Ions in Gases*; Wiley: New York, 1973.
(37) Lindinger, W.; Albritton, D. L. *J. Chem. Phys.* **1975**, *62*, 3517−3522.
(38) Kickel, B. L.; Armentrout, P. B. *J. Am. Chem. Soc.* **1995**, *117*, 764−773.
(39) Weisshaar, J. C. In *Advances in Chemical Physics*, Ng, C. Y., Baer, M., Eds.; Wiley: New York, 1992; Vol. LXXXII.
(40) Tonkyn, R.; Ronan, M.; Weisshaar, J. C. *J. Phys. Chem.* **1988**, *92*, 92−102.
(41) Hanton, S. D.; Noll, R. J.; Weisshaar, J. C. *J. Chem. Phys.* **1992**, *96*, 5176−5190.
(42) Ohanessian, G.; Brusich, M. J.; Goddard, W. A. *J. Am. Chem. Soc.* **1990**, *112*, 7179−7188.
(43) Von Helden, G.; Kemper, P. R.; Hsu, M.; Bowers, M. T. *J. Chem. Phys.* **1992**, *96*, 6591−6605.
(44) Van Koppen, P. A. M.; Kemper, P. R.; Bowers, M. T. in *Organometallic Ion Chemistry*; Freiser, B. S., Eds.; Kluwer Academic Publishers: Boston, 1996.
(45) Ohanessian, G.; Goddard, W. A., III *Acc. Chem. Res.* **1990**, *23*, 386−392.
(46) Su, T.; Chesnavich, W. J. *J. Chem. Phys.* **1982**, *76*, 5183.
(47) Hertwig, R. H.; Koch, W.; Schröder. D.; Schwarz, H.; Hrušák, J.; Schwerdtfeger, P. *J. Phys. Chem.* **1996**, *100*, 12253−12260.
(48) Schilling, B. J.; Beauchamp, J. L. *J. Am. Chem. Soc.* **1988**, *110*, 15−24.
(49) Haynes, C. L.; Armentrout, P. B. *Organometallics* **1994**, *13*, 3480−3490.
(50) Jacobsen, D. B.; Freiser, B. S. *J. Am. Chem. Soc.* **1983**, *105*, 7484−7491.